Mechanisms underlying contrast-dependent orientation selectivity in mouse V1

Wei P. Dai[a,b], Douglas Zhou[b,c,d,1], David W. McLaughlin[e,f,g,h,i,1], and David Cai[b,c,d,e,f,g,j]

[a]School of Physics and Astronomy, Shanghai Jiao Tong University, Shanghai 200240, China; [b]Institute of Natural Sciences, Shanghai Jiao Tong University, Shanghai 200240, China; [c]School of Mathematical Sciences, Shanghai Jiao Tong University, Shanghai 200240, China; [d]Ministry of Education Key Laboratory of Scientific and Engineering Computing, Shanghai Jiao Tong University, Shanghai 200240, China; [e]Courant Institute of Mathematical Sciences, New York University, New York, NY 10012; [f]Center for Neural Science, New York University, New York, NY 10012; [g]New York University Shanghai, Shanghai 200122, China; [h]NYU Tandon School of Engineering, New York University, Brooklyn, NY 11201; [i]Neuroscience Institute of NYU Langone Health, New York University, New York, NY 10016; and [j]NYUAD Institute, New York University Abu Dhabi, Saadiyat Island, Abu Dhabi, United Arab Emirates

Contributed by David W. McLaughlin, September 13, 2018 (sent for review November 2, 2017; reviewed by David Hansel and Michael P. Stryker)

Recent experiments have shown that mouse primary visual cortex (V1) is very different from that of cat or monkey, including response properties—one of which is that contrast invariance in the orientation selectivity (OS) of the neurons' firing rates is replaced in mouse with contrast-dependent sharpening (broadening) of OS in excitatory (inhibitory) neurons. These differences indicate a different circuit design for mouse V1 than that of cat or monkey. Here we develop a large-scale computational model of an effective input layer of mouse V1. Constrained by experiment data, the model successfully reproduces experimentally observed response properties—for example, distributions of firing rates, orientation tuning widths, and response modulations of simple and complex neurons, including the contrast dependence of orientation tuning curves. Analysis of the model shows that strong feedback inhibition and strong orientation-preferential cortical excitation to the excitatory population are the predominant mechanisms underlying the contrast-sharpening of OS in excitatory neurons, while the contrast-broadening of OS in inhibitory neurons results from a strong but nonpreferential cortical excitation to these inhibitory neurons, with the resulting contrast-broadened inhibition producing a secondary enhancement on the contrast-sharpened OS of excitatory neurons. Finally, based on these mechanisms, we show that adjusting the detailed balances between the predominant mechanisms can lead to contrast invariance—providing insights for future studies on contrast dependence (invariance).

orientation selectivity | contrast invariance | contrast dependence

The front end of the visual system in the cortex, the primary visual cortex (V1), has proven for cat and monkey to be appropriate for large-scale computational modeling—primarily because of the rich collection of experimental measurements on V1 that biologically constrain these models. These large-scale models have then been used to suggest potential mechanisms for various response properties in cat (or monkey) V1, such as orientation selectivity (OS) (1, 2). Individual neurons in V1 respond preferentially to the orientations of edges in the visual scene. This orientation preference is measured by the neuron's orientation tuning curve, a graph of the neuron's firing rate versus the orientation of the visual stimulus. The tuning curve is (usually) uni-modal, with a peak at "preferred orientation" (PO) and troughs at the "orthogonal orientation" (OO). Its half-width at half-maximum, the tuning width, is one measure of the neuron's OS. Although neurons' firing rates often increase with the contrast of the visual stimuli, surprisingly, the OS in cat (or monkey) is found to be approximately contrast-invariant (3, 4). Many theoretical (5–8) and experimental (9–11) works have addressed the source of this contrast invariance. In mouse, despite its poor visual acuity, neurons in V1 are surprisingly well-tuned for orientation (12–14), with tuning widths similar to those of cat or monkey. A series of experiments (13, 15, 16), as well as a behavioral vs. neuronal discrimination experiment (14), have shown that instead of contrast-invariant OS, excitatory (inhibitory) neurons in mouse V1 exhibit contrast-sharpened (broadened) OS.

Sophisticated optogenetic tools for mouse are providing even more comprehensive experimental data than are available for cat or monkey. Visual neuroscientists now have a detailed circuit structure of mouse V1 (17–21) and rich measurements of its response properties (12, 13, 22, 23). Thus, it is time for theorists to develop comprehensive large-scale models of mouse V1, which may unravel the mechanism underlying its response properties, such as the contrast-dependent OS.

There are significant hardwired differences between mouse V1 and cat (or monkey) V1, which we incorporate into our model. Neurons of mouse V1 receive only weakly tuned input (19) from the lateral geniculate nucleus (LGN); the receptive fields (RF) of this input have strongly overlapping ON and OFF subregions (15, 23), and the diameters of the LGN RFs are very large—averaging more than 10° for excitatory neurons and 20° for inhibitory neurons (23) (Fig. 1 *A*, *Top Left*), while in cat and

Significance

Recently, sophisticated optogenetic tools for mouse have enabled many detailed studies of the neuronal circuits of its primary visual cortex (V1), providing much more specific information than is available for cat or monkey. Among various other differences, they show a striking contrast dependency in orientation selectivity in mouse V1 rather than the well-known contrast invariance for cat and monkey. Constrained by the existing experiment data, we develop a comprehensive large-scale model of an effective input layer of mouse V1 that successfully reproduces the contrast-dependent phenomena and many other response properties. The model helps to probe different mechanisms based on excitation–inhibition balance that underlie both contrast dependencies and invariance, and it provides implications for future studies on these circuits.

Author contributions: W.P.D., D.Z., D.W.M., and D.C. designed research; W.P.D. performed the research; W.P.D., D.Z., D.W.M., and D.C. contributed new reagents/analytic tools; W.P.D., D.Z., D.W.M., and D.C. analyzed data; and W.P.D., D.Z., D.W.M., and D.C. wrote the paper.

Reviewers: D.H., Centre de Neurophysique, Université Paris Descartes; M.P.S., University of California San Francisco Medical Center.

The authors declare no conflict of interest.

Data deposition: The source code for our model have been deposited on GitHub (https://github.com/g13/mouseV1).

[1]To whom correspondence may be addressed. Email: david.mclaughlin@nyu.edu or zdz@sjtu.edu.cn.

This article contains supporting information online at www.pnas.org/lookup/suppl/doi:10.1073/pnas.1719044115/-/DCSupplemental.

Published online October 18, 2018.

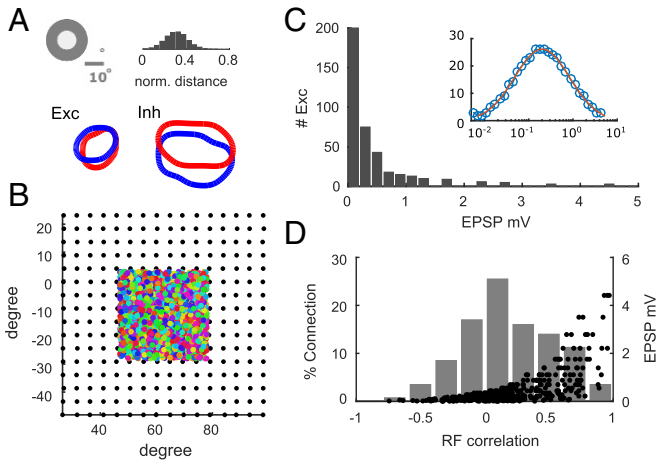

Fig. 1. Simulation setup. (*A*, *Top Left*) Typical size of an LGN RF in mouse vs. that of a monkey, a small point to the right. (*Top Right*) Gaussian distribution of normalized distance between subregions with a mean of 0.305 and SD of 0.1. (*Bottom*) Examples of inherited RF from LGN for V1 excitatory (Exc) and inhibtory (Inh) neurons with the ON subregion (red) and OFF subregion (blue). (*B*) A patch of V1 neuron (colored dots) plotted on a grid of LGN cells (black dots) in a visual field. Different colors indicate different POs. (*C*) Histogram of EPSPs to excitatory neurons with log-normal distribution. *Inset* shows the same data but with log *x* axis, with a mean of 0.45 mV and SD of 0.68 mV. (*D*) The distribution of EPSPs (dots) received by an example excitatory neuron over the pairwise RF CC distribution of its presynaptic excitatory neurons (background).

monkey the subregions are more segregated (24, 25), with diameters mostly below 1°. Cat and monkey V1 have ordered maps of PO, tiled by orientation pinwheels (26); in contrast, mouse V1 has a disordered "salt and pepper" map of PO (27). Layer 2/3 (L2/3) in cat and monkey V1 is dominated by "complex" (nonlinear) neurons (28, 29). However, in mouse, "simple" (linear) neurons make up the majority ($70 \sim 80\%$) of excitatory neurons in L2/3 and L4, and most of the inhibitory neurons are complex (12). An early lesion experiment on mouse has shown that LGN axons arborize in L2/3 as well as in L4 (30). The layer-specific data from ref. 12 also indicate that the linearity ($F1/F0$) distribution, the OS distribution, and the RF size are similar in L2/3 and L4. Taken together, the common properties shared by L2/3 and L4 in mouse provide certain justification for combining L2/3 and L4 into a single "effective layer." It is also found that the excitatory neurons selectively receive strong excitatory postsynaptic potentials (EPSPs), ~ 4.5 mV, from neurons with similar RFs (21), while an amplitude of $1 \sim 2$ mV is considered large in cat V1 (31). The inhibitory population in mouse V1 receives strong input from the LGN as shown in refs. 32 and 33, while such data are rather scarce for cat and monkey. Inhibitory neurons in mouse V1 receive strong input from cortical excitatory neurons regardless of their PO (17), and they show much poorer OS (22, 34) than the inhibitory neurons in cat or monkey V1 [but see a sharply tuned subtype (35)]. These hardwired differences suggest that different mechanisms may underlie the response properties of mouse V1 from those of cat or monkey.

Here we construct a comprehensive large-scale, biologically constrained by experimental data, model of an effective input layer of mouse V1 from which many experimentally observed response properties emerge; then we analyze in detail the contrast-sharpening (contrast-broadening) of the OS of excitatory (inhibitory) neurons and extract the underlying mechanisms from the model by probing the excitation–inhibition (E–I) balances; based on the extracted mechanisms, we further identify the adjustments to the E–I balance and the selectivity of connectivity that result in contrast invariance. Thus, with the experimentally constrained nature of the model, our result bears insights for future studies on contrast invariance and contrast dependence.

Methods

Our model consists of a grid of 16×16 LGN cells covering a visual field of $75^\circ \times 75^\circ$ and a patch of 10,800 V1 neurons in a single layer compressed from L2/3 and L4, with an effective neuronal density of $2.9 \times 10^4/\text{mm}^2$ (36). The V1 patch is a uniform mixture of a 120×72 grid of excitatory neurons and a 60×36 grid of inhibitory neurons, such that the E-I ratio is kept at 4 : 1. The model is described with sufficient details in *SI Appendix* to enable the reproduction of simulation results; the source code can be found at https://github.com/g13/mouseV1. Here we only present an overview of the model setup, emphasizing its salient features including each that distinguishes mouse V1 from that of cat or monkey, as summarized in the Introduction.

LGN Layer, Mapping to V1. The LGN input to V1 is modeled with a linear–nonlinear Poisson paradigm. Drifting sinusoidal waves with a temporal frequency of 4 Hz, a spatial frequency of 0.04 cycle per degree, and contrasts of 12.5%, 25%, 50%, and 100% are used as the external inputs to LGN. We adopt the parameters and a typical gain curve from the experiment on mouse dorsal LGN cells (37) to construct a spatiotemporal separable center-surround RF kernel and a static nonlinearity, respectively. We apply the nonlinearity on the result of the convolution of the RF kernel with the input. Its output is then used as the rate of a Poisson process from which we form the spike train inputs to V1 neurons.

Each V1 neuron is connected postsynaptically to a collection of LGN cells with two largely overlapping subregions, one of ON LGN cells and the other of OFF LGN cells. Taken together, these two subregions form the RF of the V1 neuron inherited from LGN. The extent of overlap is described by a normalized distance between the two subregions' tentative centers (see *SI Appendix*). The normalized distance has a Gaussian distribution across the population (Fig. 1 *A*, *Top Right*), whose mean and SD are derived from the experiments in refs. 19, 23. Examples of V1 neurons' RFs resulting from such connections are shown in Fig. 1 *A*, *Lower*. Notice the size difference between excitatory and inhibitory RFs, as multiple experiments have shown for mouse V1 that inhibitory neurons receive about twice the LGN input received by excitatory neurons (32, 33). To implement this experimental result, we assume the following: (*i*) an increase in LGN input to inhibitory neurons through an increase in the number of presynaptic LGN cells projecting to the inhibitory neuron (~ 30 to each inhibitory neuron, ~ 15 to each excitatory neuron), and (*ii*) the increase in LGN cells extends along the major axes of the ON and OFF subregions. We make these two detailed assumptions in the model to show a more prominent contrast-broadening effect in inhibitory neurons; however, they are not essential (see *SI Appendix*, Fig. S2).

Cortical Layer. The salt and pepper distribution of POs in mouse V1 (Fig. 1*B*) is modeled by presetting each V1 neuron's RF with a uniform distribution of POs. The probability of intracortical connections decays over distance through an isotropic Gaussian distribution for both excitatory and inhibitory neurons. Periodic boundary conditions are applied when the connection distance exceeds the boundary of the V1 patch, and all of the neurons are used in analysis. The total connection probability to an excitatory neuron is sparse—15% (20) (~ 400 *E* and ~ 100 *I* neurons). Excitatory neurons in L2/3 of mouse V1 are known to have larger probabilities to connect with excitatory neurons that share similar RFs and POs (20, 21), and a similar preferential connectivity between excitatory neurons ($E \to E$) is likely to exist in L4 as well (19). Likewise, the same connection preference has also been implied for the $I \to E$ connections by Tan et al. (38). Thus, we introduce another Gaussian distribution to capture these orientation preferential couplings to excitatory neurons (details available in *SI Appendix*). In addition to the orientation preferential connection probability, Cossell et al. (21) found the $E \to E$ connection strengths to be dependent on the pairwise correlation coefficient (CC; see *SI Appendix* for its definition) of RFs, and the EPSPs have a highly skewed distribution toward a larger amplitude (21). In this model, we implement this dependency with a log-normal distribution (Fig. 1*C*, comparable with the experiment in ref. 21; the *Inset* figure shows the same data in log-scale). One example of an excitatory neuron's presynaptic EPSP distribution for such a setup is shown in Fig. 1*D*, where the background histogram gives the distribution of RF CC with its presynaptic neurons (higher value indicates a more similar RF). Note that, although few in number, those with larger RF CC produce much larger EPSP amplitudes such that, on average, 50% of the cortical excitation is contributed by those 18% of presynaptic neurons with larger RF CC, comparable with the experiment in ref. 21.

On the other hand, the $E \to I$ connections are found experimentally to be much stronger, more numerous, and with no selectivity over orientation, as shown by Bock et al. (17). Consistently, in our model, the corresponding connection probability is set at 60% ($\sim$1000 E and $\sim$300 I neurons) and only depends on distance, with connection strength on par with the largest excitatory-to-excitatory connection strength.

Each V1 neuron is represented as a conductance-based exponential integrate-and-fire point neuron model (39) with frequency adaptation. The adaptation is modeled by a self-inhibitory conductance g_{adap} that only increases when the neuron itself fires. The voltage dynamics of the ith neuron in the kth population is thus governed by

$$\begin{aligned}\frac{dV_k^i}{dt} &= -g_{L,k}\left(V_k^i - V_L\right) + g_{L,k}\Delta_T \exp\left(\frac{V_k^i - V_T}{\Delta_T}\right)\\ &\quad + I_{syn,k}^i(t) - g_{adap}^i(t)\left(V_k^i - V_I\right),\\ I_{syn,k}^i(t) &= -\left(g_{E\to k}^i(t) + g_{LGN\to k}^i(t)\right)\left(V_k^i - V_E\right)\\ &\quad - g_{I\to k}^i(t)\left(V_k^i - V_I\right),\end{aligned} \quad [1]$$

where $k = E$ or I. $g_{L,E} = 50\ s^{-1}$ and $g_{L,I} = 70\ s^{-1}$ are the leak conductance of excitatory and inhibitory neurons, respectively. $V_L = 0$, $V_E = 2.8$, and $V_I = -0.4$ are the dimensionless reversal potentials. $\Delta_T = 0.4375$ concerns the voltage slope of spike initiation, and $V_T = 1$ is the soft threshold; the hard threshold where V_k^i is reset to V_L is set to 4.375. $I_{syn,k}^i$ is the total synaptic current, where the excitatory ($g_{E\to k}^i$), LGN ($g_{LGN\to k}^i$), and inhibitory ($g_{I\to k}^i$) conductances are summed over all spikes of the corresponding presynaptic neurons. The temporal profiles of all of the conductances are modeled by alpha functions (see *SI Appendix*). A modified Runge–Kutta scheme in ref. 40 is used in the simulation.

We use $1 - \mathrm{CV} = \left|\Sigma_j r_j e^{2i\theta_j}\right| / \Sigma_j r_j$, where CV is circular variance and r_j is the firing rate with input orientation θ_j, to describe the overall sharpness of a tuning curve (12, 13); a larger $1 - \mathrm{CV}$ indicates a sharper OS.

Results

Our effective input-layer model largely reproduces the response properties of the V1 network, including the distributions of firing rates, tuning widths, response modulation F1/F0 (simple and complex neurons), and interspike intervals. These are presented, discussed, and compared with experimental observations in *SI Appendix*. In the main text, we focus on the results of contrast-related OS properties.

Contrast Dependency. The contrast-sharpening (contrast-broadening) of OS in excitatory (inhibitory) neurons is captured by the model, as shown in Fig. 2. Fig. 2 *A* and *B* show two sets of tuning curves with various firing rate levels, for excitatory and inhibitory neurons, respectively. Both contrast-sharpening and contrast-broadening phenomena are present saliently in Fig. 2 *C* and *D*, where population-averaged tuning curves at different contrasts are normalized and aligned to the optimal input orientation for excitatory and inhibitory populations, respectively. The phenomena of contrast dependencies are also apparent in terms of $1 - \mathrm{CV}$ in Fig. 2 *E* and *F*, as the $1 - \mathrm{CV}$ distribution of excitatory and inhibitory populations are separated by the dotted contrast-invariant line.

The tuning curves of the conductances impinging on excitatory and inhibitory neurons are shown in Fig. 2 *G* and *H*, respectively, where all tuning curves are normalized to their own maxima, except the first temporal harmonic of the LGN conductance, $F1$ (magenta), which is normalized by its mean value, $F0$. The $F1$ part of the LGN conductance shows negligible signs of contrast dependency and is only weakly tuned for orientation. However, as shown in Fig. 2*G*, the tuning curves of cortical excitatory conductance (red, $g_{E\to E}$) are clearly contrast-sharpened, while the inhibitory conductance (blue, $g_{I\to E}$) is contrast-broadened, comparable with the experiment in ref. 13. Other input conductances, such as $g_{E\to I}$, are orientation-unspecific (Fig. 2*H*), which is consistent with the experiment in ref. 17 (see *SI Appendix*, Fig. S6). The magnitude of the excitatory conductance $g_{E\to I}$ (Fig. 2*I*) increases substantially with contrast, surpassing and then overwhelming the LGN conductance. This strong and orientation-unspecific cortical excitation to the inhibitory population is crucial in the model for the contrast-broadening of OS in inhibitory neurons, which then give rises to the broadening of $g_{E\to I}$ with increasing contrast.

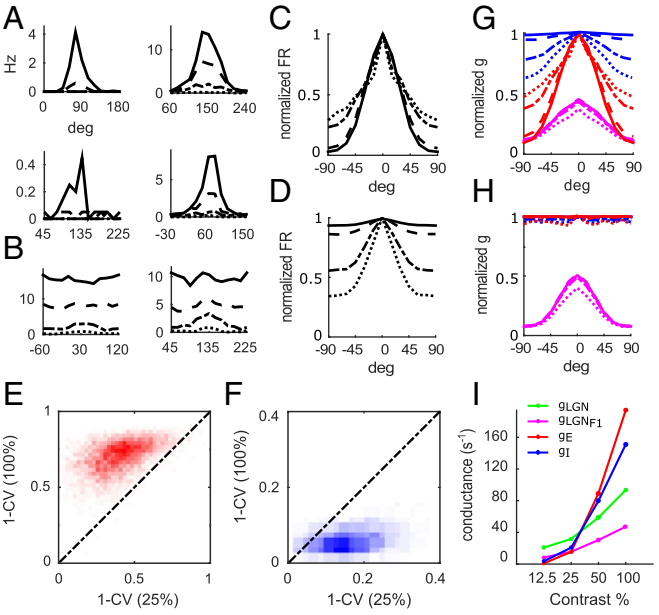

Fig. 2. Simulation results. Tuning curves of 12.5%, 25%, 50%, and 100% contrasts are in dotted, dot-dashed, dashed, and solid lines, respectively. (*A* and *B*) Examples of firing rate tuning curves of excitatory and inhibitory neurons, respectively. (*C* and *D*) Population averages of excitatory and inhibitory neurons' firing rate tuning curves, respectively. Every tuning curve is normalized by its maximum firing rate. (*E* and *F*) Heatmaps for the density distribution of $1 - \mathrm{CV}$ with contrast at 25% vs. 100% for the firing rate tuning curves of excitatory and inhibitory populations, respectively. The dot-dashed line indicates contrast-invariant OS. (*G* and *H*) Population averaged, normalized tuning curves of conductances in excitatory and inhibitory neurons, respectively. The legend follows *I*. The total LGN conductance is not shown here, since it is flat and overlapped at $y = 1$. Instead, we plot the F1 component of the LGN conductance (magenta) normalized to the F0 component. (*I*) Absolute levels of different conductances in the inhibitory population across contrasts corresponding to *H*, with averaged total LGN conductance in green.

Underlying Mechanisms. Next, we describe and analyze the mechanisms underlying the contrast dependencies in our model, as illustrated in Fig. 3*A*, where input orientations are indicated by different colors. At low contrasts, since the excitatory firing rates are low, feed-forward input (from LGN) makes up the majority of the excitation (Fig. 2*I*). Thus, the tuning curves are largely shaped by the LGN inputs, which themselves are only weakly tuned due to the strong overlap between the ON and OFF subregions. In addition, the orientation-specific $I \to E$ inhibitory connections result in weakly tuned $g_{I\to E}$ that helps to lift the cap on the excitatory firing rates at OO, while limiting the firing rate at the PO. Thus, at low contrasts, the excitatory neurons' tuning curves are relatively broad.

At higher contrasts, increased cortical firing rates cause the cortical drive to become stronger. Therefore, excitatory neurons experience enhanced cortical excitation at PO but only small increases at OO—since excitatory neurons of similar RF and PO are more likely to be connected and connected with stronger EPSPs. This orientation-specific cortical excitation raises the excitatory neurons' responses, especially at PO. Meanwhile,

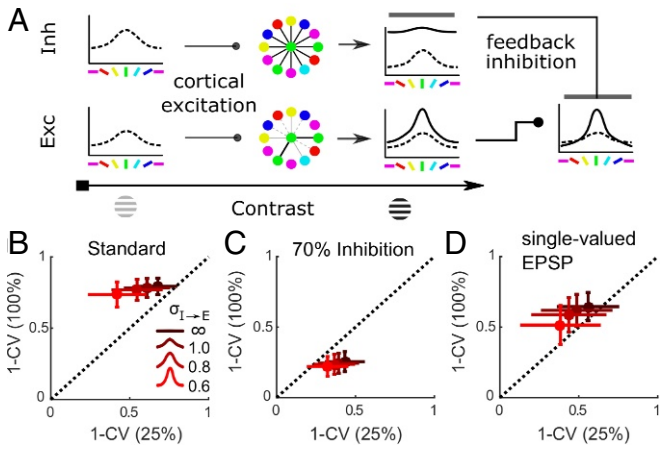

Fig. 3. Underlying mechanisms. (*A*) Diagram of the mechanism for the contrast-dependent phenomena, with excitatory sharpening on *Lower* and inhibitory broadening on *Upper*. The arrow along the *x* axis marks the direction of increasing contrast. Tuning curves at low contrast are indicated by the dotted lines, while the tuning curves at high contrast are in solid lines, and the input orientations are indicated by bars of different colors. Schematic illustrations of excitatory presynaptic connections are shown in between the tuning curves of low and high contrasts. The colored filled circle at each center is an excitatory (inhibitory) neuron of interest, and its presynaptic neurons of different POs (indicated by different colors) are connected with a different strength in dashed gray, solid gray, thin solid black, and thick solid black lines (from weak to strong). (*B*) $1-\mathrm{CV}$ value of the firing rate tuning curves for excitatory populations under 100% contrast vs. 25% contrast, with the same standard parameters used as in Fig. 2, except the SD of $I\to E$ connections, $\sigma_{I\to E}=0.6, 0.8, 1.0, \infty$, as shown in the legend (0.6 is used for Fig. 2). SDs along both axes are shown by the error bars. (*C*) Same as *B*, but with 70% cortical inhibition in excitatory neurons. Connection strengths are adjusted correspondingly. (*D*) Same as *B* but with single-valued EPSP instead of log-normal distributed EPSP.

inhibitory neurons receive much stronger cortical excitation at all orientations, which dominates the LGN input (Fig. 2*I*) and produces high inhibitory firing rates that inflict strong feedback inhibition onto excitatory neurons. This orientation-unspecific cortical excitation results in the broadened OS of inhibitory neurons, which in turn broadens the tuning curves of $g_{I\to E}$. In the meantime, this broadened feedback inhibition pulls down the excitatory neurons' responses at all orientations (more so at OO than that of low contrast). Thus, the OS of excitatory neurons is significantly sharpened.

Both the level of the inhibition ($g_{I\to E}$) and its contrast-broadened profile contribute to the contrast-sharpening of OS in excitatory neurons. To show which property of $g_{I\to E}$ contributes more, we vary the SD of the connection probability of the $I\to E$ connections, $\sigma_{I\to E}$, from 0.6 to ∞ with other parameters unchanged. $\sigma_{I\to E}$ sets the sharpness of the tuning curves of $g_{I\to E}$ at low contrast (illustrated by the legend in Fig. 3*B*), when the inhibitory firing rate is relatively selective (Fig. 2*D*). Since at higher contrast, $g_{I\to E}$ is always flat following the contrast-broadened inhibitory firing rate, the effect of the contrast-broadening of $g_{I\to E}$ is largely determined by $\sigma_{I\to E}$ at low contrast—the smaller $\sigma_{I\to E}$, the larger the effect of the contrast-broadening of $g_{I\to E}$. Thus, the case with $\sigma_{I\to E}=\infty$ represents the complete absence of contrast-broadening in $g_{I\to E}$, since it is flat across all contrasts. The simulation results in Fig. 3*B* show that all of these cases reside above the contrast-invariant line, indicating that the contrast-sharpening phenomenon exists with or without the contrast-broadening of $g_{I\to E}$. On the other hand, if we reduce the overall level of inhibition to 70% by decreasing connection strengths, while keeping the firing level relatively unchanged, none of the cases retains contrast-sharpening (Fig. 3*C*). This indicates that the level of inhibition is more relevant than the contrast-broadening of $g_{I\to E}$. However, the broadened profile of $g_{I\to E}$ does make a (secondary) contribution to the contrast-sharpening of OS in excitatory neurons, for if we quantify the contrast-sharpening effect by the distance to the contrast-invariant line, then stronger contrast-broadening of $g_{I\to E}$ does shift the OS of excitatory neurons toward the stronger contrast-sharpening effect (Fig. 3*B*). Nonetheless, this sharpening effect is not sufficient to overcome the broadening caused by a 30% decrease in the magnitude of inhibition. These results demonstrate that the level of inhibition plays a more important role than the contrast-broadening of $g_{I\to E}$ as mechanisms that underlie the contrast-sharpening of OS in excitatory neurons.

To assess the contribution of the log-normal EPSP distribution to the contrast-sharpening of OS, we set all $E\to E$ connections to have the same strength value as the mean in the original log-normal distribution. As shown in Fig. 3*D*, without the log-normal EPSP distribution, only a very weak contrast-sharpening effect exists, as the values are fairly close to the contrast-invariant line, with the error bars crossing it. Thus, the heterogeneity from the log-normal EPSP distribution is also important for the contrast-sharpening of OS in excitatory neurons, as they compensate an otherwise lower and less tuned cortical excitation. Notice that the populations with smaller $\sigma_{I\to E}$ (stronger contrast-broadening of $g_{I\to E}$) maintain their close distance to the contrast-invariant line, showing that the contrast-broadening of $g_{I\to E}$ has a much less effective role in the contrast-sharpening of OS in excitatory neurons than the standard case shown in Fig. 3*B*. Its actual cause can be attributed to both the weakened preferential excitation due to the single-valued EPSP and a major decrease in the otherwise strong feedback inhibition that is driven by the now less active excitatory neurons (see *SI Appendix* for details).

To summarize, the preferential $E\to E$ connections and their stronger connection strengths, together with strong feedback inhibition, are the primary mechanisms by which the model achieves contrast-sharpening of OS in the excitatory population, while the nonpreferential $E\to I$ connections lead to contrast-broadening of OS in inhibitory neurons.

Discussion

In this work, we construct a large-scale effective input-layer model for mouse V1 under the constraints from experimental data. The model successfully reproduces response properties

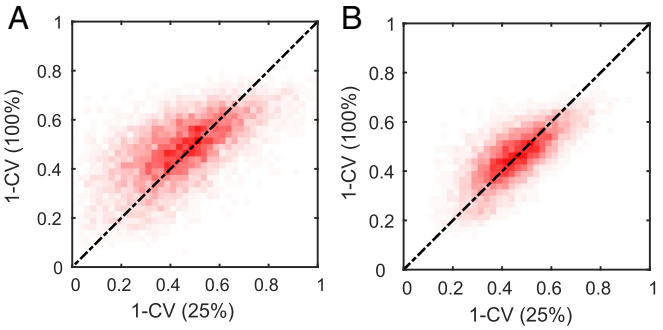

Fig. 4. Contrast-invariant excitatory OS. $1-CV$ value under 100% contrast vs. under 25% contrast for the excitatory firing rates. The dotted lines indicate contrast-invariant OS. (*A*) The log-normal EPSP distribution is replaced with a single-valued EPSP, the same as in Fig. 3*D*; $\sigma_{E\to E}=0.65$ (0.5 in standard case) and $\sigma_{I\to E}=1.0$ are used, and the connection strengths are not changed. (*B*) Eighty percent inhibition also achieves contrast-invariant OS without changes in the connection profile but only with changes in connection strengths ($\sigma_{I\to E}=1.0$).

experimentally observed for mouse V1, including contrast-sharpening (contrast-broadening) of OS in excitatory (inhibitory) populations. We show that strong, highly preferential ($E \to E$) excitation, strong feedback ($I \to E$) inhibition, and strong orientation-unspecific cortical ($E \to I$) excitation are the primary mechanisms underlying the contrast-dependent phenomena in the model and that the effects of the contrast-broadening of $g_{I \to E}$ are secondary for the contrast-sharpening of OS in excitatory neurons.

Previously, theoretical modeling works on mouse V1 of Hansel and Van Vreeswijk (41) and Sadeh and Rotter (42) have throughly discussed the mechanisms of emergent OS from a randomly connected network without an orientation map. These studies focused on contrast invariance and revealed how a small input bias in orientation can be amplified in a balanced network or an inhibition-dominated network, respectively. Another study by Roy et al. (43) explores the parameter space to reproduce experimentally observed OS distributions in mouse V1 at a fixed contrast, and they find it necessary to have orientation preferential $E \to E$ connections. In contrast, we constrain our model by experimental observations of mouse V1 on various input properties (17, 19, 23, 32, 33)—for example, a highly skewed distribution of $E \to E$ connection strengths (21), which depend on pairwise correlation of RFs—and investigate contrast-dependent OS (13) and its possible underlying mechanisms. A simulation-assisted analysis, as discussed in *SI Appendix*, provides additional intuition about the mechanisms underlying the model's performance.

There is an informative analogy between our mouse V1 model and models of monkey V1 (1, 44) where neurons closer to pinwheel centers are more sharply tuned than neurons farther from the centers—because neurons near the centers receive inhibition from the nearby inhibitory neurons with all POs, while those far from the center are inhibited by nearby neurons with similar POs. This process of the distance-dependent "center-broadening" of inhibition (mediated by the inhibitory conductances) resulting in the "center-sharpening" of OS is very similar to the process of the contrast-broadening of $g_{I \to E}$ helping to enhance the contrast-sharpening of OS in excitatory neurons in our mouse model. Consistently, when inhibition is less dominant in the monkey V1 models, center-sharpening of OS is also lessened (44), just as shown by our analysis on the effects of contrast-broadening of $g_{I \to E}$.

Limitations. First, the gain curves of the excitatory neurons are relatively too low at low contrast compared with experimental observations. Second, our model's $1 - CV$ distribution for excitatory neurons represents only a sharply tuned subset of the neurons in the experiments (12, 13) rather than the entire distribution; moreover, in our model, the OS of the excitatory population is substantially sharper than the experimental measurements (19, 45). In an effort to address these two limitations, we have incorporated synaptic depression into the LGN input of the model. We show in *SI Appendix* that this modified model has very similar contrast-dependent phenomena and the same major underlying mechanisms as in our original model but with more realistic gain curves and OS. However, in this modified model, the contrast-broadening of $g_{I \to E}$ conductance is significantly reduced.

Contrast Invariance, With or Without Ordered Maps of PO. The pinwheel-like ordered map of PO in cat (or monkey) V1 versus the random salt and pepper map of PO in mouse V1 is one of the most striking differences between the two anatomically. However, topographically, they have similar selective connectivities based on PO. In monkey, the ordered map of PO implicitly creates selective connectivity since nearby neurons are more likely to be connected than distant neurons and nearby neurons naturally have similar POs in the map. In mouse, an explicit selective $E \to E$ connectivity based on similar POs replaces the implicit selectivity for monkey.

It seems that the explicit connectivity in mouse V1, contributing substantially in producing contrast-sharpening, may be stronger than the implicit connectivity in an ordered map of PO, even though the neuronal density of macaque V1 is about 2.5 times that of a rodent (46), which together with the pooling of neurons (with similar POs) in the ordered map of PO provides a larger reservoir of potential preferential connections than is available to excitatory neurons in mouse V1, which have to search through the uniformly distributed PO. Thus, it is very likely that the much stronger bias in the $E \to E$ connection strengths (21) in mouse V1 overcompensates for the low availability of preferential connections to help achieve contrast-sharpening of OS in excitatory neurons.

Thus, one may wonder whether contrast invariance can be observed if one were to correct the overcompensation of $E \to E$ orientation preference. Indeed, if we moderately weaken the preference of $E \to E$ connections by increasing $\sigma_{E \to E}$ from 0.5 to 0.65 and reduce the strength of their EPSPs (through a single-valued EPSP distribution), contrast invariance in the excitatory population is obtained, as shown in Fig. 4*A*. A major consequence of this relative decrease in excitation is a resulting decrease in feedback inhibition to the excitatory neurons, which decreases sharpening. Therefore, an alternative way to achieve contrast-invariant OS in the model (without explicitly modifying the preferential excitatory connections) is to directly decrease the overall level of inhibition as hinted by Fig. 3*C*. To do this, we follow the scheme used for Fig. 3*C*, keeping the $I \to I$ connection strength constant and decreasing the other connection strengths. Note that we only decrease them moderately so that the overall inhibition is weakened only by $\sim 20\%$, in contrast to the 30% used for Fig. 3*C*. Again, contrast-invariant OS of excitatory neurons is obtained, as shown in Fig. 4*B*.

With these two examples, we demonstrate two ways to produce contrast-invariant OS in the excitatory neurons. Importantly, both methods adjust the E-I balance, by decreasing either the preferential cortical excitation or the feedback inhibition—the two primary and interrelated mechanisms that underlie the contrast-sharpening of OS in excitatory neurons. Thus, with reasonable variability of E-I balances, it is possible that both contrast-invariant and contrast-sharpening of excitatory neurons are actually present in mouse V1, which suggests further experimental studies on contrast dependence of OS in mouse and bears an implication for the understanding of contrast invariance of other species in general.

ACKNOWLEDGMENTS. We thank Louis Tao for initial discussions of this work, and the two referees for their helpful reviews. This research was carried out on the High Performance Computing resources at New York University Abu Dhabi. This work was supported by National Science Foundation in China Grants 11671259, 11722107, 91630208, and 31571071 (to D.Z. and D.C.) and by NYU Abu Dhabi Institute Grant G1301 (to W.P.D., D.Z., and D.C.).

1. McLaughlin D, Shapley R, Shelley M, Wielaard DJ (2000) A neuronal network model of macaque primary visual cortex (V1): Orientation selectivity and dynamics in the input layer 4Cα. *Proc Natl Acad Sci USA* 97:8087–8092.
2. Chariker L, Shapley R, Young LS (2016) Orientation selectivity from very sparse lgn inputs in a comprehensive model of macaque V1 cortex. *J Neurosci* 36:12368–12384.
3. Sclar G, Freeman RD (1982) Orientation selectivity in the cat's striate cortex is invariant with stimulus contrast. *Exp Brain Res* 46:457–461.
4. Skottun BC, Bradley A, Sclar G, Ohzawa I, Freeman RD (1987) The effects of contrast on visual orientation and spatial frequency discrimination: A comparison of single cells and behavior. *J Neurophysiol* 57:773–786.

5. Ben-Yishai R, Bar-Or RL, Sompolinsky H (1995) Theory of orientation tuning in visual cortex. *Proc Natl Acad Sci USA* 92:3844–3848.
6. Troyer TW, Krukowski AE, Miller KD (2002) Lgn input to simple cells and contrast-invariant orientation tuning: An analysis. *J Neurophysiol* 87:2741–2752.
7. Lauritzen TZ, Miller KD (2003) Different roles for simple-cell and complex-cell inhibition in V1. *J Neurosci* 23:10201–10213.
8. Finn IM, Priebe NJ, Ferster D (2007) The emergence of contrast-invariant orientation tuning in simple cells of cat visual cortex. *Neuron* 54:137–152.
9. Nelson S, Toth L, Sheth B, Sur M (1994) Orientation selectivity of cortical neurons during intracellular blockade of inhibition. *Science* 265:774–777.
10. Ferster D, Chung S, Wheat H (1996) Orientation selectivity of thalamic input to simple cells of cat visual cortex. *Nature* 380:249–252.
11. Chung S, Ferster D (1998) Strength and orientation tuning of the thalamic input to simple cells revealed by electrically evoked cortical suppression. *Neuron* 20:1177–1189.
12. Niell CM, Stryker MP (2008) Highly selective receptive fields in mouse visual cortex. *J Neurosci* 28:7520–7536.
13. Li Yt, et al. (2012) Broadening of inhibitory tuning underlies contrast-dependent sharpening of orientation selectivity in mouse visual cortex. *J Neurosci* 32:16466–16477.
14. Long M, Jiang W, Liu D, Yao H (2015) Contrast-dependent orientation discrimination in the mouse. *Sci Rep* 5:15830.
15. Liu Bh, et al. (2010) Intervening inhibition underlies simple-cell receptive field structure in visual cortex. *Nat Neurosci* 13:89–96.
16. Liu Bh, et al. (2011) Broad inhibition sharpens orientation selectivity by expanding input dynamic range in mouse simple cells. *Neuron* 71:542–54.
17. Bock DD, et al. (2011) Network anatomy and in vivo physiology of visual cortical neurons. *Nature* 471:177–182.
18. Ko H, et al. (2011) Functional specificity of local synaptic connections in neocortical networks. *Nature* 473:87–91.
19. Lien AD, Scanziani M (2013) Tuned thalamic excitation is amplified by visual cortical circuits. *Nat Neurosci* 16:1315–1323.
20. Ko H, et al. (2013) The emergence of functional microcircuits in visual cortex. *Nature* 496:96–100.
21. Cossell L, et al. (2015) Functional organization of excitatory synaptic strength in primary visual cortex. *Nature* 518:399–403.
22. Kerlin AM, Andermann ML, Berezovskii VK, Reid RC (2010) Broadly tuned response properties of diverse inhibitory neuron subtypes in mouse visual cortex. *Neuron* 67:858–871.
23. Liu Bh, et al. (2009) Visual receptive field structure of cortical inhibitory neurons revealed by two-photon imaging guided recording. *J Neurosci* 29:10520–10532.
24. Jin J, Wang Y, Swadlow HA, Alonso JM (2011) Population receptive fields of on and off thalamic inputs to an orientation column in visual cortex. *Nat Neurosci* 14:232–238.
25. Mata ML, Ringach DL (2005) Spatial overlap of on and off subregions and its relation to response modulation ratio in macaque primary visual cortex. *J Neurophysiol* 93:919–928.
26. Ohki K, et al. (2006) Highly ordered arrangement of single neurons in orientation pinwheels. *Nature* 442:925–928.
27. Bonin V, Histed MH, Yurgenson S, Reid RC (2011) Local diversity and fine-scale organization of receptive fields in mouse visual cortex. *J Neurosci* 31:18506–18521.
28. Gilbert CD (1977) Laminar differences in receptive field properties of cells in cat primary visual cortex. *J Physiol* 268:391–421.
29. Ringach DL, Shapley RM, Hawken MJ (2002) Orientation selectivity in macaque V1: Diversity and laminar dependence. *J Neurosci* 22:5639–5651.
30. Frost DO, Caviness VS (1980) Radial organization of thalamic projections to the neocortex in the mouse. *J Comp Neurol* 194:369–393.
31. Stratford K, Tarczy-Hornoch K, Martin K, Bannister N, Jack J (1996) Excitatory synaptic inputs to spiny stellate cells in cat visual cortex. *Nature* 382:258–261.
32. Cruikshank SJ, Urabe H, Nurmikko AV, Connors BW (2010) Supplemental figures from "Pathway-Specific feedforward circuits between Thalamus and neocortex revealed by selective optical stimulation of axons". *Neuron* 65:230–245.
33. Kloc M, Maffei A (2014) Target-specific properties of Thalamocortical synapses onto layer 4 of mouse primary visual cortex. *J Neurosci* 34:15455–15465.
34. Sohya K, Kameyama K, Yanagawa Y, Obata K, Tsumoto T (2007) GABAergic neurons are less selective to stimulus orientation than excitatory neurons in layer II/III of visual cortex, as revealed by in vivo functional Ca2+ imaging in transgenic mice. *J Neurosci* 27:2145–2149.
35. Runyan CA, et al. (2010) Response features of parvalbumin-expressing interneurons suggest precise roles for subtypes of inhibition in visual cortex. *Neuron* 67:847–857.
36. Herculano-Houzel S, Watson C, Paxinos G (2013) Distribution of neurons in functional areas of the mouse cerebral cortex reveals quantitatively different cortical zones. *Front Neuroanat* 7:35.
37. Grubb MS, Thompson ID (2003) Quantitative characterization of visual response properties in the mouse dorsal lateral geniculate nucleus. *J Neurophysiol* 90:3594–3607.
38. Tan AYY, Brown BD, Scholl B, Mohanty D, Priebe NJ (2011) Orientation selectivity of synaptic input to neurons in mouse and cat primary visual cortex. *J Neurosci* 31:12339–12350.
39. Brette R, Gerstner W (2005) Adaptive exponential integrate-and-fire model as an effective description of neuronal activity. *J Neurophysiol* 94:3637–3642.
40. Shelley MJ, Tao L (2001) Efficient and accurate time-stepping schemes for integrate-and-fire neuronal networks. *J Comp Neuro* 11:111–119.
41. Hansel D, van Vreeswijk C (2012) The mechanism of orientation selectivity in primary visual cortex without a functional map. *J Neurosci* 32:4049–4064.
42. Sadeh S, Rotter S (2015) Orientation selectivity in inhibition-dominated networks of spiking neurons: Effect of single neuron properties and network dynamics. *Plos Comput Biol* 11:e1004045.
43. Roy D, et al. (2013) Afferent specificity, feature specific connectivity influence orientation selectivity: A computational study in mouse primary visual cortex. arXiv:1301.0996. Preprint, posted January 6, 2013.
44. Kang K, Shelley M, Sompolinsky H (2003) Mexican hats and pinwheels in visual cortex. *Proc Natl Acad Sci USA* 100:2848–2853.
45. Pattadkal JJ, Mato G, van Vreeswijk C, Priebe NJ, Hansel D (2018) Emergent orientation selectivity from random networks in mouse visual cortex. *Cell Rep* 24:2042–2050.e6.
46. Srinivasan S, Carlo CN, Stevens CF (2015) Predicting visual acuity from the structure of visual cortex. *Proc Natl Acad Sci USA* 112:7815–7820.